Reports in Mechanical Engineering
Vol. 2, No. 1, 2021, pp. 77-85
ISSN: 2683-5894, DOI: https://doi.org/10.31181/rme200102077v

BCC lattice cell structural characterization

Andrea Alaimo[1], Federico Marino[1] and Stefano Valvano[1]
[1]University Kore of Enna, Italy

Article info

Article history:

Received: 13 March 2021
Revised: 2 April 2021
Accepted: 19 April 2021

Keywords:

FEM
Lattice
BCC
Struts
Additive

ABSTRACT

In this work, a numerical characterization of BCC lattice cells is performed through the use of an homogenization approach. The main goal is to establish a relationship among those properties and the relative density of the cubic unit cell. The BCC cell struts diameter are the inputs parameters of the homogenization analysis campaing in order to vary the relative density of the unit cell. A linear periodic condition has been applied to the model in order to simulate a clear probing situation. Traction load tests are used in order to evaluate the Young modulus and the Poisson coefficient, differently a pure shear load case is employed for the evaluation of the shear modulus. Hence the final results will be presented in a graphic visualization.

Corresponding Author:

Stefano Valvano,
Faculty of Engineering and Architecture,
University Kore of Enna
Cittadella Universitaria, 94100, Enna, Italy.
E-mail:
stefano.valvano@unikore.it

1 Introduction

Nowadays the additive manufacturing technique Guo and Leu (2013), Bikas et al. (2016), Kumar and Kruth (2010), Vayre et al. (2012), Rajaguru et al. (2020), Gardan (2016) have been rather studied and applied to different engineering fields such as: civil, bio-mechanical, automotive and aerospace Bici et al. (2018), Liu et al. (2017), Kamal and Rizza (2019), Najmon et al. (2019), Kumar and Nair (2017), Rawal et al. (2013), Shapiro et al. (2016), Uriondo et al. (2015) even if many aspects that comprises it are still not properly understood. In this large portion of fields, low-density and relatively complex geometries are needed in order to fulfill the requirements. One of the main advantages of this manufacturing technique is to deal with lattice structures made by unit cells Maskery et al. (2018), Hazeli et al. (2019), Jin et al. (2019), Aboudi and Gilat (2005), Wallach and Gibson (2001), Shen et al. (2010), Liu et al. (2006), Zok et al. (2004). For instance Lei et al. (2019) made a study concerning about the practical influence of the geometrical properties of two similar cells, the BCC and the BCCZ one, showing how these geometrical parameters afflict the mechanical behavior of the whole structure. The strategy of placing side-by-side these cells allow to reach the macroscopic shape that's needed, still working with the inner components of the main structure Lei et al. (2019), Deshpande and Fleck (2001), Wang et al. (2003), Kooistra et al. (2004), Queheillalt and Wadley (2005a), Queheillalt and Wadley (2005b). Speaking of which is one of the main problems connected to the usage of AM, we'll focus on the influence of the cell's behavior when the relative density is forced to vary Duan et al. (2020) Xiao et al. (2018) Jin et al. (2018) Dumas et al. (2017). In fact the behavior of unit cells is different in respect to the particular configuration. Basically we can distinguish between bending dominated and stretching dominated cells, as introduced by Ashby (2006), which properties are directly proportional to the already cited relative density that is defined as:

$$\frac{\rho}{\rho_s} \tag{1}$$

where in this case ρ is the density of the considered BCC cell, and ρ_s is the density of the full equivalent shape. However the present work is made in order to characterize a symmetric cubic unit cell, hence an isotropic condition is provided by this configuration.

2 Lattice unit cell

As we said before, the cell we chose for the characterization is a BCC, that falls into the bending dominated behavior ones. This division in respect of mechanical behavior is the same introduced by (Ashby 2006), using the Maxwell's stability criterion Deshpande et al. (2001) defined by the so called Maxwell's number:

$$M = b - 2j + 3 = 0 \tag{2}$$

which in our case, the three-dimensional one, becomes:

$$M = b - 3j + 6 = 0 \tag{3}$$

where b is the strut's number of the considered cell and j is the number of frictionless joints which the cell is made by. Using Equation 3, various cases can be distinguish, that is:

- M<0 where the structure has one or more degrees of freedom hence not providing any stiffness in these directions, that characterize the bending dominated behavior structures
- M=0 where all members of the structure carry tension or compression, that leads to the stretching dominated behavior structures
- M>0, that leads to the so called self-stress structures.

According to this criterion, we can state that the BCC cell we treated has $M < 0$, so it's classified as a bending dominated structure. Hence, a simple analytic law links the relative density with the relative Young's modulus of a bending dominated structure, namely:

$$\frac{E_c}{E_s} \propto \left(\frac{\rho_c}{\rho_s}\right)^2 \tag{4}$$

which in our case E_c and E_s are the cell's Young's modulus and bulk modulus respectively, in the same way ρ_c and ρ_s are the cell and bulk densities respectively. Equation 4 permits to affirm that when the cell density tends to the bulk one, as a consequence, the cell and bulk Young's moduli tend to be equal, as follow:

$$\rho_c = \rho_s \Leftrightarrow E_c = E_s \tag{5}$$

2.1 Geometry

A visualization of the BCC unit cell chosen for the characterization is shown in Figure 1, in particular it shows a 1mm strut condition, that is, a cell which has a 1mm diameter struts. Moreover the side of the cube which the cell is made into is 10mm. Whilst the length of the cell is set frozen, the strut's diameter is forced to vary in order to cover a range of densities, so to follow Equation 4 hence allowing us to extract the varying law for the Young's modulus. The same setup is used to establish the Poisson's coefficient and the shear modulus of the unit cell.

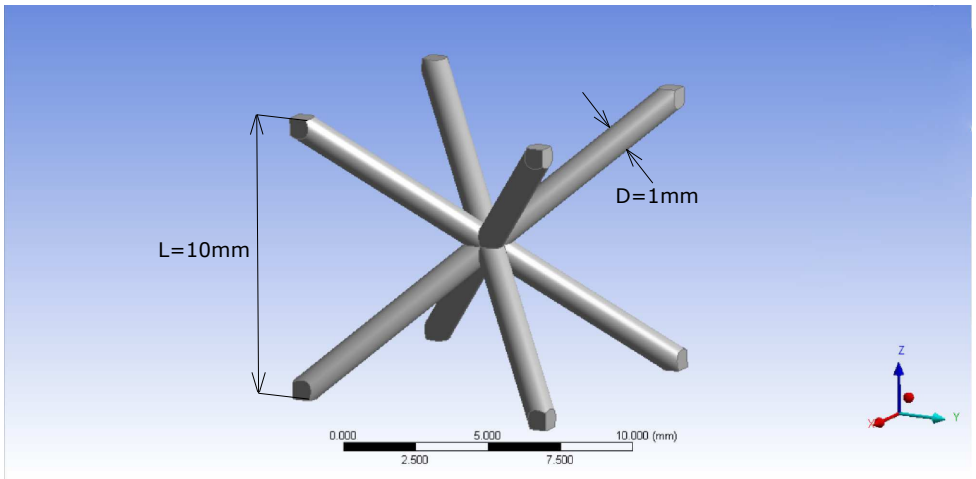

Figure 1. Implemented BCC cell with specified geometrical lengths

The relative density has been varied through the configurations depicted in Figure 2a and Figure 2b. Respectively those setups are referred to a corresponding relative density of 0.0033% and 0.9862%. Overall, 16 strut's configurations have been implemented to cover up a well-spaced range of densities.

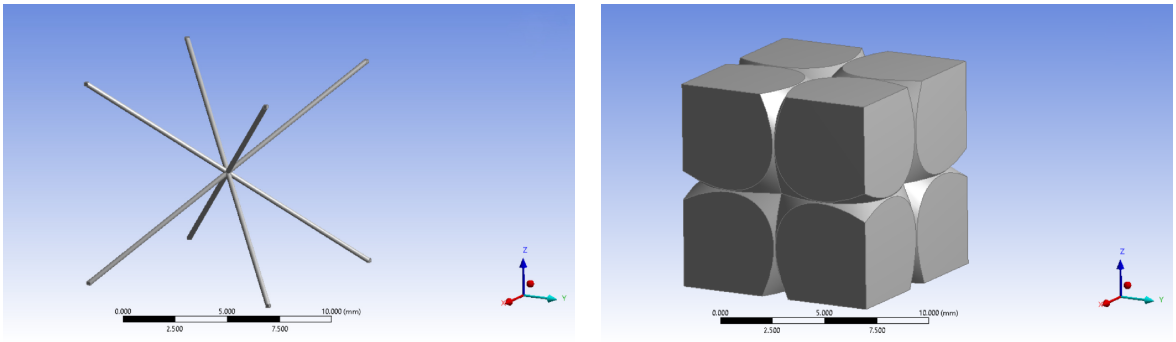

(a) (b)

Figure 2. BCC cell with 0.25mm strut diameter a, and 7mm strut diameter b

3 Numerical simulations

The software used in this characterization was ANSYS, in its mechanical environment. CAD models of the cells have been implemented into ANSYS' Design Modeler environment, hence a direct implementation was made. In order to automatize the process, parametric simulations were conduced, that is, the strut's diameter has been varied introducing a corresponding Design Point for each value. Eventually, for each Design Point we defined also a parametric mesh column, in order to fit the best element's mesh size for each Design Point, so to establish the best compromise either for simulation velocity and data precision.

3.1 FEM model

As a first approach analysis, no structured mesh were built, instead an automatic meshing method was chosen. As result, tetrahedral elements were used such the best-fitting for this problem. An estimation of the element's number is not reported since different struts configurations leads to a considerable varying of element's number.

3.2 Linear periodic condition

We've remarked several times that the usage of this type of lattice cells is currently the basic idea beyond AM processes. Hence, numerical simulations must fulfill a set of conditions that best-fits the given problem. If a single cell analysis had been conducted, the model wouldn't have got an acceptable precision. In fact, since we're trying to model a structural-behavior, we can't avoid to consider the whole interaction among cells. As a consequence, a linear periodic region have been set in the X and Y directions by using constraint equations. The goal is to couple the displacements between the two cell's side, so to simulate an interaction between adjacent cells in reality. The defined constraint equations are one for each direction, hence providing:

$$X_{pos} = X_{neg} + X_{PN} \tag{6}$$
$$Y_{pos} = Y_{neg} + Y_{PN} \tag{7}$$

where X_{pos}, X_{neg}, Y_{pos} and Y_{neg} are the displacements of the X- and Y- oriented faces of the cell respectively to the relative position along either the positive X and Y axes and negative X and Y axes respectively, moreover, PN is a random node defined by the ANSYS linear periodic symmetry rule. The implemented linear periodic condition have been depicted in Figure 3.

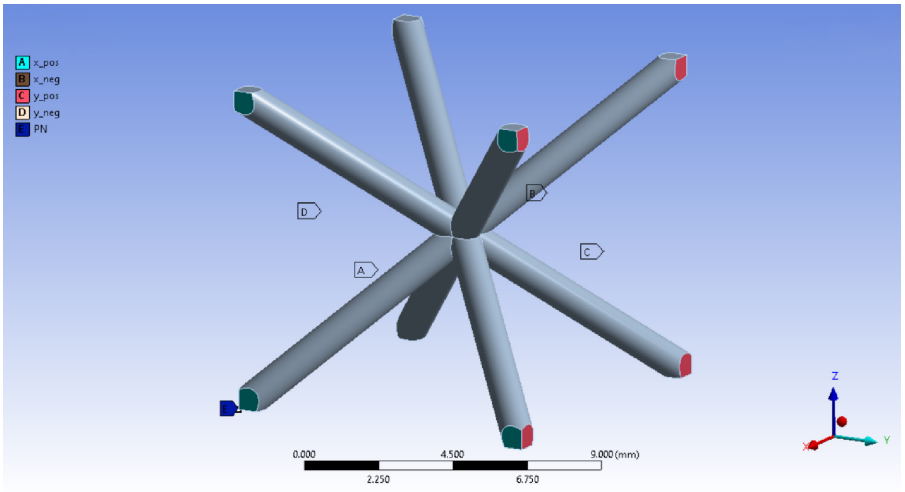

Figure 3. Applied linear periodic condition

3.3 Uni-axial traction setup

The setup we're going to enunciate has been chosen in order to allow to probe two magnitudes at once, namely either the one used for computing the Young's modulus and the Poisson's coefficient. We should clarify that since an isotropic condition have been introduced, we consider:

$$E_x = E_y = E_z = E, \qquad \nu_{xy} = \nu_{xz} = \nu_{yz} = \nu, \qquad G_{xy} = G_{xz} = G_{yz} = G. \tag{8}$$

As we see in Figure 4 a simple support condition has been imposed to the base, in particular the displacement along the Z axis of the four faces, which the cell's base is made by, has been set null. Whilst a traction condition has been set on the upper four faces by using a 1mm imposed displacement along the Z axis.

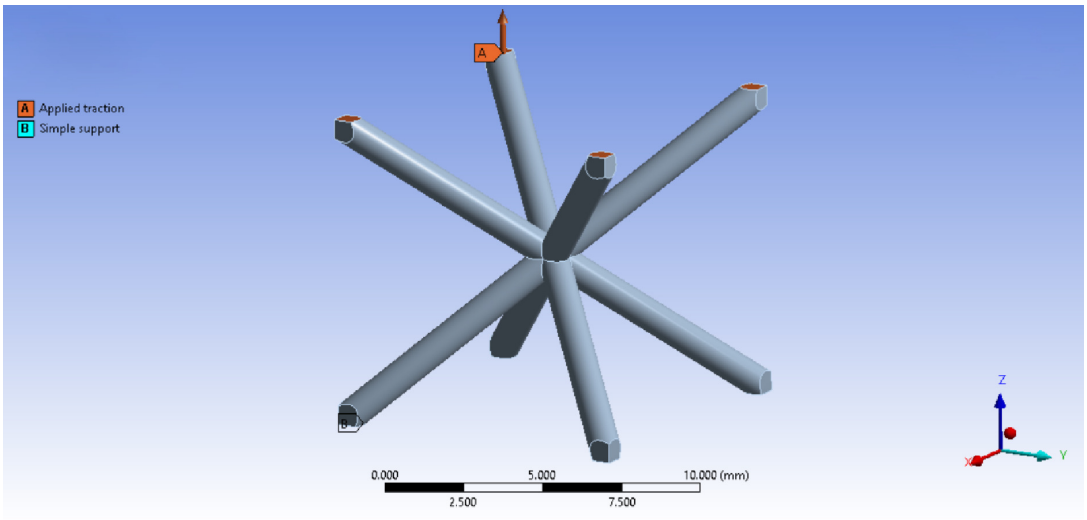

Figure 4. Uniaxial load condition

This load configuration, coupled with the applied linear periodic condition, allows to probe:

- The force reaction F_r of the cell's base along the Z direction, that allowed us to obtain the Young's modulus
- The deformations of the cell's side, that allowed us to extract the Poisson's coefficient.

In order to obtain the Young's modulus, we must use the tension definition that is:

$$\sigma_z = \frac{F_r}{A_c} \tag{9}$$

where A_c is the full shape base area, hence by the mean of the generalized Hooke law we obtain the Young's modulus that is:

$$\sigma_z = E\epsilon_z \qquad \Rightarrow \qquad E = \frac{\sigma_z}{\epsilon_z} \tag{10}$$

where ϵ_z is known since the cell's length and the value of the imposed displacement are known. For the Poisson's coefficient we must apply the well known definition of strain for example along the X axis (since we're in an isotropic condition), thus using the Poisson's coefficient definition:

$$\nu = -\frac{\epsilon_{transverse}}{\epsilon_{axial}} = -\frac{\epsilon_x}{\epsilon_z} \tag{11}$$

it is possible to obtain two of the three searched mechanical properties.

3.4 Shear setup

This setup was made in order to find the shear modulus. A representation of the load condition is depicted in Figure 5. In order to compute the shear modulus, the symmetry condition has been changed. It has been reduced to an 1D linear periodic condition, precisely along the X axis direction. On the upper faces of the cells, a 1mm displacement toward the Y axis has been imposed, while the displacement along the Z axis was set null. On the lower faces only the X axis displacement component has been set non-null. Lastly, an additional condition has been imposed, in particular the displacement along the Z axis of all Y-oriented faces was set null, in order to reproduce a pure-shear load configuration. According to this, the force reaction F_s along the Y axis has been probed, thus the definition of shear stress was applied, leading to:

$$\tau = \frac{F_s}{A_c} \tag{12}$$

similar to Equation 9, the angular displacement was computed using:

$$\gamma = \frac{D}{L} \tag{13}$$

where D corresponds to the 1mm imposed displacement and L is the cells length. Hence the shear modulus was computed using the shear-equivalent Hooke law:

$$\tau = G\gamma \qquad \Rightarrow \qquad G = \frac{\tau}{\gamma} \tag{14}$$

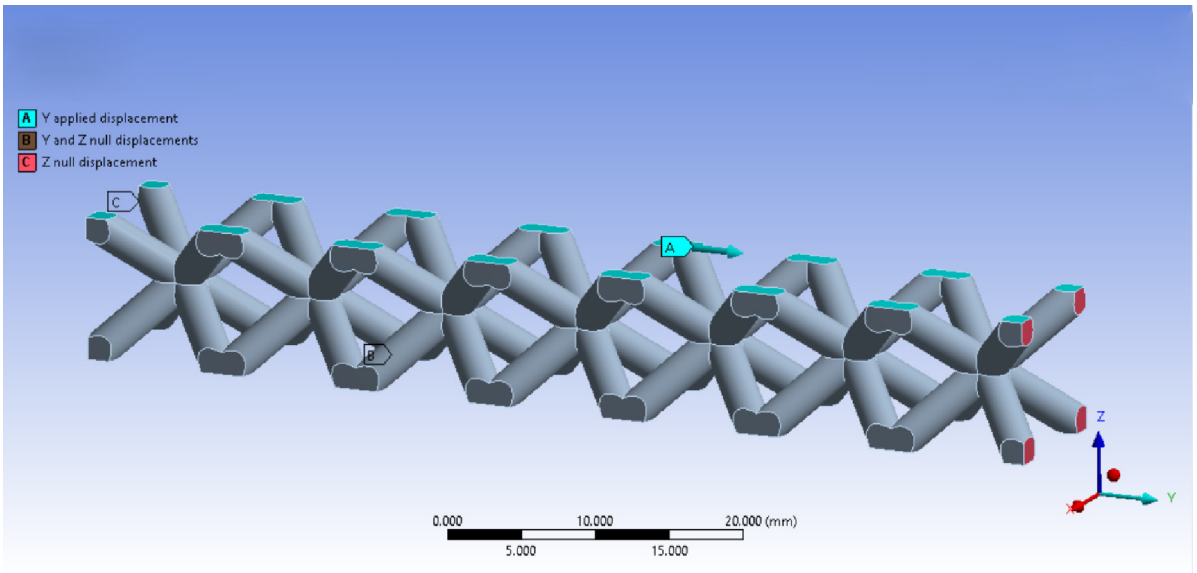

Figure 5. Shear load condition

3.5 Convergence on the cell's number

A study about the cell's number has been conducted in order to find an acceptable configuration based on the cell's number along the load axis, that is the Z axis for the Young's modulus and the Poisson's coefficient setups and the Y axis for the shear modulus setup. For the Young and Poisson setups, it has been found that a single cell setup was enough to guarantee a relative error roughly around 2%, as presented in Table 1. As this is a first order analysis, an error of roughly 2% is reputed acceptable. For the shear setup, a different condition has been applied,

that is a major number of cells has been used in order to obtain an acceptable error around 3%. The analysis has been pulled over to using seven cells so to obtain the maximal admissible error, as presented in Table 2. The error was computed by taking as reference the value which corresponds to the major cell's number, referred to the ith configuration, that is:

$$Err(E_i) = \frac{E_i - E_{ref}}{E_{ref}} \cdot 100 \tag{15}$$

where $Err(E_i)$ is the error computed for the ith cells configuration and E_{ref} is the Young's modulus for the reference cells configuration.

Table 1. Relative errors for the convergence analysis about the cell's number in the Young and Poisson setups

Cell's number	E	Error(E) %	ν	Error(ν) %
3	1.1638E+09		0.44070	
2	1.1645E+09	0.057	0.44069	0.003
1	1.1385E+09	2.178	0.44125	0.124

Table 2. Relative errors for the convergence analysis about the cell's number in the shear setup

Cell's number	G	Error(G) %
7	2.5229E+09	
6	2.4573E+09	2.597
5	2.3664E+09	6.202
4	2.2305E+09	11.590
3	2.0121E+09	20.244
2	1.6343E+09	35.220
1	1.1385E+09	54.873

As presented in tables above, a difference of 2.178% had been already found between the single cell configuration and the three cells configuration in the Young setup, which for our approximation was considered acceptable. A minor error was computed for the Poisson setup, which was considerably below 1%, thus satisfying the approximation. Lastly, for the shear setup, an acceptable error was found only using the seven cells configuration, that provided a difference of 2.597% between the six cell's configuration. Thus that configuration have been chosen for the characterization analyses presented below.

4 Results

As said before, all configurations showed upon were repeated for increasing levels of relative density $\frac{\rho}{\rho_s}$. All numerical results have been plotted in a graphical visualization, precisely the Young's modulus, the Poisson's coefficient and the shear modulus are presented respectively in Figure 6, Figure 7 and Figure 8. For the Young's modulus graph, the ideal bending dominated behavior and the stretching dominated behavior described by Ashby (2006) have been plotted too. From Figure 6, the relative Young's modulus tends to one as the relative density tends to one, as described in Equation 5. Concerning the Poisson's coefficient graph, a similar logic was followed so to compare the cell's Poisson coefficient with the bulk one. Lastly the same logic was applied for the shear modulus, hence providing slightly as a similar trend as the Young's modulus.

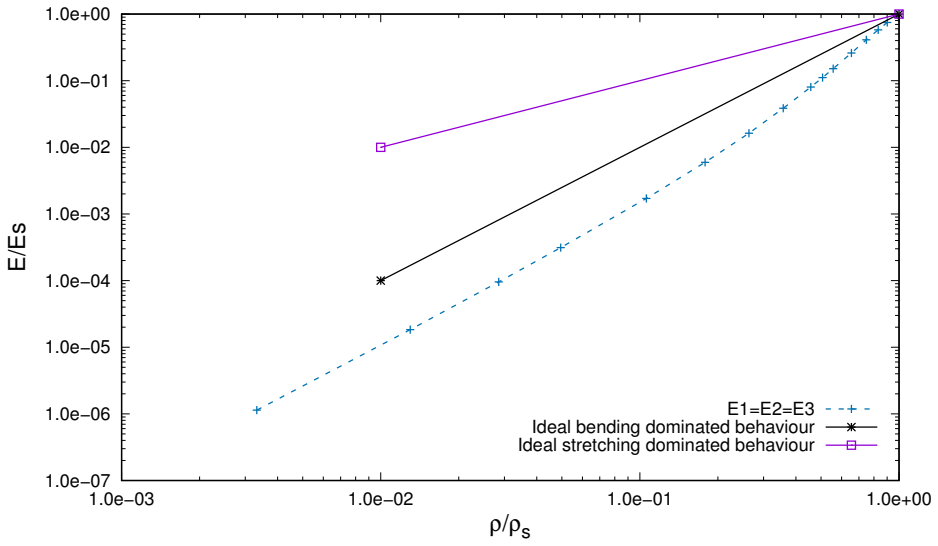

Figure 6. Relative Young's modulus against relative density

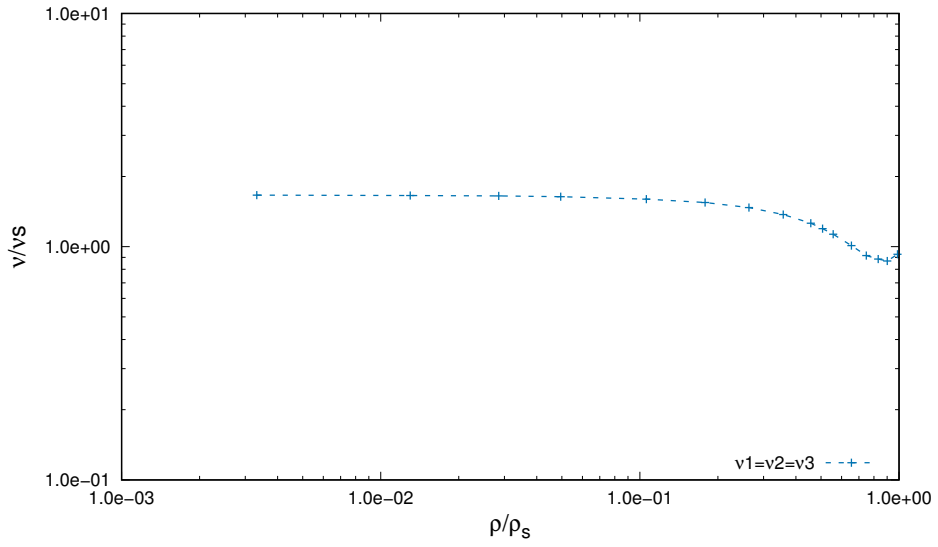

Figure 7. Relative Poisson's coefficient against relative density

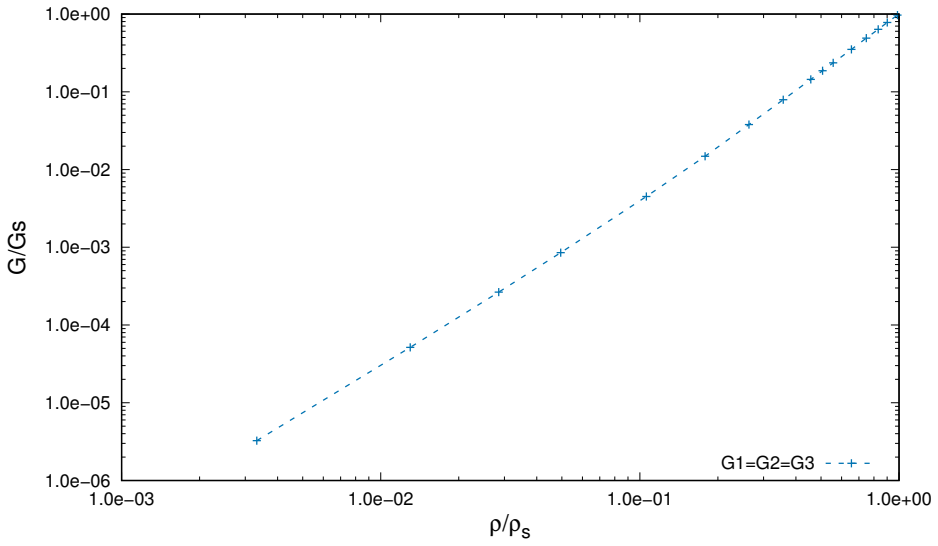

Figure 8. Relative shear modulus against relative density

5 Conclusions

In this paper a characterization of a BCC lattice unit cell, made especially for AM processes, has been conducted. Firstly the attention has been focused on the field which these type of geometries are used. Then, the simple rule which links the relative Young's modulus and the relative density has been enunciated. Thereafter the cell's geometry has been described and the parameters which typify it have been declared. A brief explanation about the relative density variation during the analyses has been provided, showing also two limit cases of the less-dense cell and the more-dense cell. Moreover, the numerical simulations settings have been described, by specifying firstly the employed mesh, then the applied linear periodic condition and finally the uni-axial traction setup and the shear setup. Furthermore, a convergence analysis has been presented in order to find the best cell configuration that fits the load conditions. By the mean of the two previously described setups, the probing of the magnitudes leads to find, using the generalized classic and shear-valid Hooke law, the values of E and G. The definition of the Poisson's coefficient was applied to compute ν instead. These three properties were further divided by the correspondent bulk value, so to obtain the relative ratios. All these three ratios have been plotted against the relative density of the cells, in respect to the various cases, in order to obtain the associated trends. Lastly it has to be noticed that this was a first-approach analysis, in fact further studies will be made in order to pass from an isotropic condition to an orthotropic one, using a non-cubic cell shape.

References

Aboudi J and Gilat R (2005) Micromechanical analysis of lattice blocks. *International journal of solids and structures* 42(15): 4372–4392.

Ashby MF (2006) The properties of foams and lattices. *Philosophical Transactions of the Royal Society A: Mathematical, Physical and Engineering Sciences* 364(1838): 15–30.

Bici M, Brischetto S, Campana F, Ferro CG, Seclì C, Varetti S, Maggiore P and Mazza A (2018) Development of a multifunctional panel for aerospace use through slm additive manufacturing. *Procedia CIRP* 67: 215–220.

Bikas H, Stavropoulos P and Chryssolouris G (2016) Additive manufacturing methods and modelling approaches: a critical review. *The International Journal of Advanced Manufacturing Technology* 83(1-4): 389–405.

Deshpande VS, Ashby MF and Fleck NA (2001) Foam topology: bending versus stretching dominated architectures. *Acta materialia* 49(6): 1035–1040.

Deshpande VS and Fleck NA (2001) Collapse of truss core sandwich beams in 3-point bending. *International Journal of Solids and Structures* 38(36-37): 6275–6305.

Duan S, Xi L, Wen W and Fang D (2020) Mechanical performance of topology-optimized 3d lattice materials manufactured via selective laser sintering. *Composite Structures* 238: 111985.

Dumas M, Terriault P and Brailovski V (2017) Modelling and characterization of a porosity graded lattice structure for additively manufactured biomaterials. *Materials & Design* 121: 383–392.

Gardan J (2016) Additive manufacturing technologies: state of the art and trends. *International Journal of Production Research* 54(10): 3118–3132.

Guo N and Leu MC (2013) Additive manufacturing: technology, applications and research needs. *Frontiers of Mechanical Engineering* 8(3): 215–243.

Hazeli K, Babamiri BB, Indeck J, Minor A and Askari H (2019) Microstructure-topology relationship effects on the quasi-static and dynamic behavior of additively manufactured lattice structures. *Materials & Design* 176: 107826.

Jin N, Wang F, Wang Y, Zhang B, Cheng H and Zhang H (2019) Failure and energy absorption characteristics of four lattice structures under dynamic loading. *Materials & Design* 169: 107655.

Jin X, Li GX and Zhang M (2018) Optimal design of three-dimensional non-uniform nylon lattice structures for selective laser sintering manufacturing. *Advances in Mechanical Engineering* 10(7): 1687814018790833.

Kamal M and Rizza G (2019) Design for metal additive manufacturing for aerospace applications. In: *Additive manufacturing for the aerospace industry*. Elsevier, pp. 67–86.

Kooistra GW, Deshpande VS and Wadley HNG (2004) Compressive behavior of age hardenable tetrahedral lattice truss structures made from aluminium. *Acta Materialia* 52(14): 4229–4237.

Kumar LJ and Nair CGK (2017) Current trends of additive manufacturing in the aerospace industry. In: *Advances in 3D printing & additive manufacturing technologies*. Springer, pp. 39–54.

Kumar S and Kruth JP (2010) Composites by rapid prototyping technology. *Materials & Design* 31(2): 850–856.

Lei H, Li C, Meng J, Zhou H, Liu Y, Zhang X, Wang P and Fang D (2019) Evaluation of compressive properties of slm-fabricated multi-layer lattice structures by experimental test and μ-ct-based finite element analysis. *Materials & Design* 169: 107685.

Liu R, Wang Z, Sparks T, Liou F and Newkirk J (2017) Aerospace applications of laser additive manufacturing. In: *Laser additive manufacturing*. Elsevier, pp. 351–371.

Liu T, Deng ZC and Lu TJ (2006) Design optimization of truss-cored sandwiches with homogenization. *International Journal of Solids and Structures* 43(25-26): 7891–7918.

Maskery I, Aremu AO, Parry L, Wildman RD, Tuck CJ and Ashcroft IA (2018) Effective design and simulation of surface-based lattice structures featuring volume fraction and cell type grading. *Materials & Design* 155: 220–232.

Najmon JC, Raeisi S and Tovar A (2019) Review of additive manufacturing technologies and applications in the aerospace industry. *Additive manufacturing for the aerospace industry* : 7–31.

Queheillalt DT and Wadley HNG (2005a) Cellular metal lattices with hollow trusses. *Acta Materialia* 53(2): 303–313.

Queheillalt DT and Wadley HNG (2005b) Pyramidal lattice truss structures with hollow trusses. *Materials Science and Engineering: A* 397(1-2): 132–137.

Rajaguru K, Karthikeyan T and Vijayan V (2020) Additive manufacturing–state of art. *Materials today: proceedings* 21: 628–633.

Rawal S, Brantley J and Karabudak N (2013) Additive manufacturing of ti-6al-4v alloy components for spacecraft applications. In: *2013 6th international conference on recent advances in space technologies (RAST)*. IEEE, pp. 5–11.

Shapiro AA, Borgonia JP, Chen QN, Dillon RP, McEnerney B, Polit-Casillas R and Soloway L (2016) Additive manufacturing for aerospace flight applications. *Journal of Spacecraft and Rockets* : 952–959.

Shen Y, McKown S, Tsopanos S, Sutcliffe CJ, Mines RAW and Cantwell WJ (2010) The mechanical properties of sandwich structures based on metal lattice architectures. *Journal of Sandwich Structures & Materials* 12(2): 159–180.

Uriondo A, Esperon-Miguez M and Perinpanayagam S (2015) The present and future of additive manufacturing in the aerospace sector: A review of important aspects. *Proceedings of the Institution of Mechanical Engineers, Part G: Journal of Aerospace Engineering* 229(11): 2132–2147.

Vayre B, Vignat F and Villeneuve F (2012) Metallic additive manufacturing: state-of-the-art review and prospects. *Mechanics & Industry* 13(2): 89–96.

Wallach JC and Gibson LJ (2001) Mechanical behavior of a three-dimensional truss material. *International Journal of Solids and Structures* 38(40-41): 7181–7196.

Wang J, Evans AG, Dharmasena K and Wadley HNG (2003) On the performance of truss panels with kagome cores. *International Journal of Solids and Structures* 40(25): 6981–6988.

Xiao Z, Yang Y, Xiao R, Bai Y, Song C and Wang D (2018) Evaluation of topology-optimized lattice structures manufactured via selective laser melting. *Materials & Design* 143: 27–37.

Zok FW, Waltner SA, Wei Z, Rathbun HJ, McMeeking RM and Evans AG (2004) A protocol for characterizing the structural performance of metallic sandwich panels: application to pyramidal truss cores. *International Journal of Solids and Structures* 41(22-23): 6249–6271.